AIP | Physics of Fluids

Strong and weak, unsteady reconfiguration and its impact on turbulence structure within plant canopies

Ying Pan, Elizabeth Follett, Marcelo Chamecki, and Heidi Nepf

Citation: Physics of Fluids (1994-present) **26**, 105102 (2014); doi: 10.1063/1.4898395
View online: http://dx.doi.org/10.1063/1.4898395
View Table of Contents: http://scitation.aip.org/content/aip/journal/pof2/26/10?ver=pdfcov
Published by the AIP Publishing

PHYSICS OF FLUIDS **26**, 105102 (2014)

Strong and weak, unsteady reconfiguration and its impact on turbulence structure within plant canopies

Ying Pan,[1,a)] Elizabeth Follett,[2] Marcelo Chamecki,[1] and Heidi Nepf[2]
[1]*Department of Meteorology, The Pennsylvania State University, University Park, Pennsylvania 16802, USA*
[2]*Department of Civil and Environmental Engineering, Massachusetts Institute of Technology, Cambridge, Massachusetts 02139, USA*

(Received 24 March 2014; accepted 6 October 2014; published online 21 October 2014)

Flexible terrestrial and aquatic plants bend in response to fluid motion and this reconfiguration mechanism reduces drag forces, which protects against uprooting or breaking under high winds and currents. The impact of reconfiguration on the flow can be described quantitatively by introducing a drag coefficient that decreases as a power-law function of velocity with a negative exponent known as the Vogel number. In this paper, two case studies are conducted to examine the connection between reconfiguration and turbulence dynamics within a canopy. First, a flume experiment was conducted with a model seagrass meadow. As the flow rate increased, both the mean and unsteady one-dimensional linear elastic reconfiguration increased. In the transition between the asymptotic regimes of negligible and strong reconfiguration, there is a regime of weak reconfiguration, in which the Vogel number achieved its peak negative value. Second, large-eddy simulation was conducted for a maize canopy, with different modes of reconfiguration characterized by increasingly negative values of the Vogel number. Even though the mean vertical momentum flux was constrained by field measurements, changing the mode of reconfiguration altered the distribution, strength, and fraction of momentum carried by strong and weak events. Despite the differences between these two studies, similar effects of the Vogel number on turbulence dynamics were demonstrated. In particular, a more negative Vogel number leads to a more positive peak of the skewness of streamwise velocity within the canopy, which indicates a preferential penetration of strong events into a vegetation canopy. We consider different reconfiguration geometry (one- and two-dimensional) and regime (negligible, weak, and strong) that can apply to a wide range of terrestrial and aquatic canopies. © *2014 AIP Publishing LLC*. [http://dx.doi.org/10.1063/1.4898395]

I. INTRODUCTION

Over the past two decades, the quantification and understanding of land-surface fluxes from vegetated surfaces such as forests and crops has been the focus of great research efforts. These studies have been motivated by the important exchanges of latent heat, water vapor, and carbon dioxide that take place at the canopy-atmosphere interface. These fluxes between the terrestrial vegetation and the atmosphere impact micro and mesoscale meteorology, regional and global climate change, carbon balance and cycling, as well as hydrology.[1,2] Fluxes of trace gases and aerosols at the canopy-atmosphere interface also determine the important role of vegetated surfaces on the removal of air pollutants (e.g., tropospheric ozone,[3,4] heavy metals,[5] and aerosols[6]). Transport of biogenic particles emitted from forests and crops such as pollens,[7] seeds,[8] and spores[9] also play an important role in ecological and agricultural processes. In aquatic systems, turbulent transport at the top of submerged

a)Author to whom correspondence should be addressed. Electronic mail: yyp5033@psu.edu

vegetation may influence the availability of nutrients within the canopy as well as the release of seeds from the vegetation. In addition, the penetration of turbulence through the canopy to the bed determines the likelihood of sediment resuspension, an important feedback to vegetation health.[10,11] Specifically, resuspension negatively impacts light availability for photosynthesis and associated erosion may destabilize shoots. Dense canopies that reduce near-bed turbulence can enhance the supply of nutrients to the plants by promoting the retention of nutrient-rich fine sediment and organic matter.[12] From a fluid dynamical perspective, all these exchanges are driven by the complex turbulent flow field produced by the mechanical interactions between the flow and canopy elements. Thus, understanding these interactions and the properties of the turbulent flow produced at this interface is of great importance in all these fields.

When flow passes through vegetation canopies, surface forces acting on the interfaces between flow and canopy elements remove momentum and dissipate the kinetic energy of the flow. The bulk effect of these exchanges is a drag force acting on the mean flow within the canopy layer. For canopies of sufficient density, the discontinuity of drag at the top of the canopy leads to an inflectional mean velocity profile with the inflection point located near the canopy top. This velocity profile has a similar shape to that in a free shear layer, that is, a mixing layer formed between two uniform, parallel streams of different velocities.[13] The inflectional mean velocity profile triggers instabilities and coherent eddies within the canopy shear layer similar to the Kelvin-Helmholtz (KH) instabilities and coherent eddies observed in a free shear layer.[13] These canopy-scale coherent structures (denoted as "KH coherent structures" hereafter) dominate the transport of momentum from above the canopy to the canopy layer. For example, observations of aquatic[14] and terrestrial canopies[15] demonstrated that 80%–90% of the time-mean downward momentum transport ($\overline{u'w'} < 0$) occurred within short, intense events that occupied only 25%–35% of total time. The dominating events occurred at time-intervals consistent with the passage of the KH vortices. Here, the overbar denotes the time-average, and the primes denote instantaneous deviations, defined as $u'(t) = u(t) - \overline{u}$ and $w'(t) = w(t) - \overline{w}$, for streamwise ($u$) and vertical ($w$) velocities, respectively. Scalar flux at the canopy-free flow interface has also been linked to the passage of KH vortices in both aquatic[16] and terrestrial canopies.[17] Because of the importance of these coherent structures to the exchange of momentum and scalars, it is vital that their intensity and depth of penetration into the canopy be properly modeled.

Typically, a strong sweep ($u' > 0$, $w' < 0$) is observed as the leading edge of these coherent structures pass, and a weaker ejection ($u' < 0, w' > 0$) occurs as the trailing edge passes.[18] Physically, sweeps represent the vertical transport of fluid parcels with high momentum downward towards a boundary near which there is a region of lower average momentum, while ejections represent the vertical transport of fluid parcels with low momentum upward into a region of higher average momentum. Both sweeps and ejections result in a net downward flux of momentum ($u'w' < 0$). Many studies within a variety of real and model canopies have observed non-zero velocity skewness, specifically $Sk_u > 0$ and $Sk_w < 0$, indicating the prevalence of events with strong positive streamwise velocity ($u' > 0$) and strong negative vertical velocity ($w' < 0$), i.e., sweeps. This implication is consistent with the idea that flux into the canopy is dominated by the canopy-scale coherent structures described above. Here, the values of velocity skewness are calculated as $Sk_u = \overline{u'^3}/\sigma_u^3$ and $Sk_w = \overline{w'^3}/\sigma_w^3$, where $\sigma_u = \sqrt{\overline{u'^2}}$ and $\sigma_w = \sqrt{\overline{w'^2}}$ are the standard deviation of streamwise and vertical velocities, respectively. Reproducing velocity skewness (Sk_u and Sk_w) as well as the momentum flux transported by sweeps and ejections is therefore the basic requirement for proper modeling of canopy-scale coherent structures. However, existing third-order closure models[19] and large-eddy simulation (LES) models[20–25] have underestimated velocity skewness (Sk_u and Sk_w) as well as the ratio between momentum flux transported by sweeps and ejections by more than 50%. Recent work has shown that including a model that represents the effects of plant reconfiguration (the bending of plant stems, branches, leaves, etc.) on the flow field greatly reduces these under-predictions.[26]

Both terrestrial and aquatic plants take advantage of elastic reconfiguration to reduce drag forces and avoid uprooting or breaking under high winds and currents.[27] The impact of reconfiguration on the drag force has been described by a modification to the quadratic drag law, which can be

modeled by introducing the Vogel number B. Specifically, the drag force $F_D \propto U^{2+B}$, with U a characteristic velocity scale acting on the plant element.[27,28] It is sometimes convenient in modeling to transfer the velocity dependence to the drag coefficient, i.e., we write $F_D \propto C_D U^2$, with $C_D \propto U^B$. In the asymptotic regime of negligible reconfiguration, $B \to 0$, and the quadratic increase of drag with velocity is recovered. In the asymptotic regime of strong reconfiguration, dimensional analysis balancing drag force and the plant's internal resistance to bending suggests specific values of B.[29,30] For linear elastic bending, $B = -2/3$, if reconfiguration is associated with the loss of one characteristic length, such as the bending of a beam or a rectangular plate along a single axis, and $B = -4/3$, if reconfiguration leads to the loss of two characteristic lengths, such as the crumpling of a paper or the rolling of a disk into a cone. For some aquatic plants, the primary restoring force is buoyancy, rather than rigidity. If buoyancy alone is considered as the restoring force $B = -4/3$; and the inclusion of buoyancy in addition to rigidity as restoring forces delays the asymptotic regime of strong reconfiguration to higher values of fluid velocity.[31] These theoretical models predict drag forces in good agreement with laboratory measurements of fibers in soap films,[32] rectangular plates in a wind tunnel,[33] and model seagrass blades in water.[31] The range $-2/3 \lesssim B \lesssim 0$ is also in rough agreement with many measured values for natural canopies in which one-dimensional (1D) bending is observed.[28,30,34] For example, de Langre *et al.* reported $B = -0.52$ to -0.80,[30] and Albayrak *et al.* reported $B = -0.5$ to -0.7.[34] Harder *et al.* observed two regimes of behavior for the giant reed (*Arundo donax L.*).[35] For wind speeds up to 1 m s^{-1}, little bending occurred, and the drag force was approximately quadratic ($B \approx 0$), as expected for an unyielding object. However, for wind speeds above 1.5 m s^{-1}, significant bending occurred, and the observed $B = -0.7$ was consistent with the scaling for a reconfigured beam ($B = -2/3$).

Although most previous studies have focused on time-averaged flow conditions and the associated mean reconfiguration,[30,34] some studies report instantaneous relationships between velocity and reconfiguration.[35,36] Indeed, the phenomena of *honami* and *monami* (progressive waves of canopy bending) are examples of plants bending in response to the passage of individual canopy-scale coherent eddies.[37,38] We hypothesize that the reconfiguration of plants at time-scales comparable to individual KH eddies can preferentially enhance the penetration of strong events into a vegetation canopy because the plants yield more to strong events. Specifically, we propose that the drag coefficient responds to the instantaneous velocity, $\boldsymbol{u} = (u, v, w)$ (a vector consisting of streamwise, spanwise, and vertical components), such that the characteristic velocity $U = |\boldsymbol{u}|$ and $C_D \propto U^B$ will be smaller for stronger events (higher $|\boldsymbol{u}|$). Note $|\boldsymbol{u}|$ is statistically positively correlated with its streamwise component, u, so that in general stronger events have higher u. The canopy-drag length-scale, $L_c \propto (C_D a)^{-1}$, describes the penetration of turbulent momentum flux into the canopy,[39,40] where a is the frontal canopy area per volume. If stronger events (higher u) experience a smaller $C_D \propto U^B$, then they can penetrate a greater distance into the canopy before being arrested by drag, compared to weaker events (smaller u). This impact of plant flexibility should be evident in the skewness of the streamwise and vertical velocities (Sk_u and Sk_w, respectively), which are statistical measures of bias toward larger events.

In this paper, we consider two case studies that examine the connection between reconfiguration and turbulence structure within a canopy, focusing on skewness as an indicator for bias toward large events. First, we consider a flume experiment with a model seagrass meadow. As flow speed over the meadow increases, both the mean and unsteady reconfiguration increase. We consider how these changes in reconfiguration are connected with both the magnitude and vertical position of the peak skewness, using expected changes in $C_D \propto U^B$ based on a force balance for individual model blades.[31] Second, we investigate the effects of different modes and degrees of reconfiguration on turbulence statistics using a LES for a maize canopy, in which reconfiguration is parameterized using a range of Vogel numbers. With mean vertical momentum flux constrained by field experimental data, increasingly negative B shifts the magnitude and vertical position of peak skewness, alters the stress fractions carried by strong events, and changes the distribution of stress fractions carried by sweeps ($u' > 0$, $w' < 0$) and ejections ($u' < 0$, $w' > 0$). These case studies suggest that the proper modeling of turbulence in plant canopies requires that instantaneous reconfiguration be incorporated into models through the use of a velocity-dependent drag coefficient.

II. RECONFIGURATION AND SKEWNESS IN A MODEL SEAGRASS

In this section, we consider a model seagrass meadow that is dynamically and geometrically similar to *Zostera marina*.[14] The measurements are interpreted through the lens of a recent theoretical model that predicts the impact of mean reconfiguration on the drag experienced by individual seagrass blades.[31] We propose that the mean reconfiguration model can be used to infer the impact of instantaneous reconfiguration associated with the arrival of individual turbulent events. It is important to note that, for aquatic plants, buoyancy, in addition to rigidity and drag, can influence plant posture in flow, because the material density of many aquatic plants is below that of water (e.g., seagrass blade density is 700 kg m^{-3}),[41] compared to typical coastal water densities of 1015 kg m^{-3} (Atlas of the Oceans, NOAA). In addition, aquatic plants often have small gas filled chambers, used to enhance buoyancy and maintain upright postures.[42,43] Luhar and Nepf extended previous work on reconfiguration by considering buoyancy, drag, and rigidity together.[31] They quantified the steady reconfiguration under steady (time-average) velocity $\overline{u}$, using an effective blade length, l_e, which represents the length of a rigid, vertical blade that generates the same horizontal drag (F_D) as a flexible blade of total length l. For blade width, b, and fluid density, ρ, the effective blade length (l_e) is given by the following definition:

$$F_D = \frac{1}{2}\rho C_D^o b l_e U^2. \tag{1}$$

In Eq. (1), the drag coefficient is assumed to be a constant, which is denoted by the superscript "o." Also note that, for generality, we use the characteristic velocity scale U, which in this section refers to the time-averaged velocity $\overline{u}$. Luhar and Nepf[31] used a numerical model to predict the total drag on a single blade (F_D), and from this they extract the ratio l_e/l as a function of the mean velocity $\overline{u}$. As velocity increased, the blade bent over further in the streamwise direction, which decreased the frontal area and also created a more streamlined shape. Both effects are reflected in the decreasing value of l_e/l. Many previous studies characterized reconfiguration of aquatic vegetation through changes in the drag coefficient,[44] for which the total drag is, $F_D = (1/2)\rho C_D b l U^2$, with C_D a function of U. Equating this drag expression to Eq. (1), one can show that $l_e/l = C_D/C_D^o \propto U^B$, and we see that the dependence of l_e/l on U can be expressed through the Vogel exponent B.

Blade posture in flow is governed by two parameters. The Cauchy number, Ca, describes the ratio of the drag force to the restoring force due to rigidity. The dimensionless buoyancy, R_B, describes the ratio of restoring forces due to buoyancy and rigidity

$$Ca = \frac{1}{2}\frac{\rho C_D^o b U^2 l^3}{EI}, \tag{2}$$

$$R_B = \frac{\Delta\rho g b t l^3}{EI}. \tag{3}$$

Here, $\Delta\rho$ is the difference in density between the fluid and the blade, g is the gravitational acceleration, E is the elastic modulus, and $I = bt^3/12$ is the second moment of area, with t the blade thickness. Because these two parameters control the blade posture in flow (i.e., the degree of bending), they also predict the dependence $l_e/l = C_D/C_D^o$, as described by Luhar and Nepf.[31] For example, Fig. 1(a) depicts the dependence of C_D/C_D^o for $R_B = 0$ (no buoyancy) and $R_B = 6.4$ (the dimensionless buoyancy of the model seagrass). For the lowest values of Ca, the blade remains essentially upright (negligible reconfiguration). Consistent with this posture, the drag is quadratic with U, i.e., $C_D/C_D^o \approx 1$ and $B \approx 0$, similar to the response of the giant reed at low wind speed.[35] The main impact of buoyancy is to delay the onset of blade reconfiguration, i.e., buoyant blades remain upright at higher velocities, which extends the range of Ca for which $B \approx 0$. For $Ca > 100$, strong reconfiguration occurs (Fig. 1(c)), and the effective length-scale over which drag occurs (l_e) is comparable to the length-scale over which bending occurs (l_b). For this degree of reconfiguration, specifically $l_b = l_e$, the balance of drag to the restoring force due to rigidity produces the scaling $l_e/l = Ca^{-1/3}$, $B = -2/3$, as previously derived by Alben *et al.*[29] The drag coefficient ratio (C_D/C_D^o) displays this dependency in Fig. 1(a) for $Ca > 100$. In the regime of strong reconfiguration ($Ca > 100$), buoyancy plays a

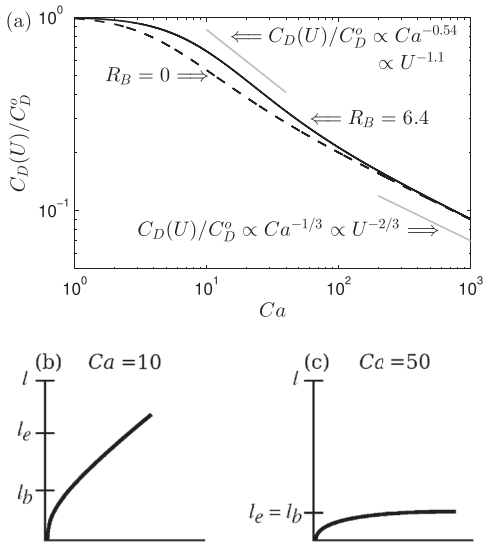

FIG. 1. (a) Dependence of normalized drag coefficient $C_D(U)/C_D^o$ with Cauchy number Ca for a simplified dense canopy flow profile, with buoyancy parameter $R_B = 6.4$ (black solid line; see Ghisalberti and Nepf[14]) and $R_B = 0$ (black dashed line). Grey solid lines with Vogel numbers $B = -1.1$ and $B = -2/3$ are noted for reference. The maximum Vogel exponent ($B = -1.1$) occurs in the weak reconfiguration regime ($Ca = 10$–50), in which the blades bend over length-scale l_b, but experience drag over length-scale $l_e > l_b$, as demonstrated with the corresponding blade posture (b). For strong reconfiguration ($Ca > 100$), as demonstrated with the corresponding blade posture (c), $l_e = l_b$, which leads to $B = -2/3$, as described by Alben *et al.*[29] This figure is a revised version of Fig. 2(c) in M. Luhar and H. M. Nepf, "Flow-induced reconfiguration of buoyant and flexible aquatic vegetation," Limnol. Oceanogr. **56**, 2003–2017 (2011). Copyright 2014 Association for the Sciences of Limnology and Oceanography, Inc.[31]

negligible role in plant posture, so that the scaling $C_D/C_D^o \propto Ca^{-1/3}$ is observed for all values of R_B (also discussed by Luhar and Nepf[31]). Finally, for weak reconfiguration, associated with intermediate values of Ca (≈10–50), the blade is only slightly bent. In this posture (Fig. 1(b)), the effective length-scale for drag (l_e) is greater than the length-scale over which bending occurs (l_b) so that a balance of drag to rigidity yields the scaling $l_e/l = C_D/C_D^o = Ca^{-1/3}\,(l_e/l_b)^2$, with $l_e/l_b > 1$. In this regime, as the velocity increases the blade progressively bends further, so that l_e/l_b decreases with increasing Ca, until $l_e/l_b \to 1$, at which point the regime of strong reconfiguration is reached. Within the weak reconfiguration regime, $(l_e/l_b)^2 \sim Ca^m$, and thus $l_e/l = Ca^{-(1/3+m)}$, $B = -(2/3 + 2m)$, so that B is most negative in the weak reconfiguration regime. In other words, for a blade geometry (i.e., bending in one dimension) the deviation from the quadratic drag response is greatest in the regime of weak reconfiguration. For example, in Fig. 1(a) the maximum slope occurs at $Ca = 21$, with $C_D/C_D^o = Ca^{-0.54}$ (i.e., $B = -1.1$). Similarly, a maximum in $-B$ was also observed at the transition between negligible and strong reconfiguration of deforming plates and disks.[33] Finally, although the curves in Fig. 1(a) strictly describe steady reconfiguration under time-mean flow, we propose that the curves can be used to interpret the impact of reconfiguration on the drag experienced by individual sweeps penetrating the canopy. We anticipate that the highest skewness values will be observed in the weak reconfiguration regime, for which B is the most negative, creating the greatest bias for strong events. This could have important implications for suspended sediment within the canopy, because the penetration of individual strong events may resuspend more material than more persistent but weaker turbulence.

A. Experimental design

The effect of reconfiguration was evaluated by comparing the behavior of a single meadow of flexible blades at six flow rates (runs F1–F6 in Ghisalberti and Nepf[14]), which resulted in different levels of both mean and unsteady reconfiguration. Each model plant was constructed of a wooden

dowel stem (1.5 cm high) and six blades ($l = 20.3$ cm, $b = 3.8$ mm, $t = 0.20$ mm) cut from low-density polyethylene (LDPE) film ($E = 3.0 \times 10^8$ Pa, $EI = 7.5^{-7}$ N m^2, and density $\rho_s = 920$ kg m^{-3}). The model plants were designed to be dynamically and geometrically similar to eelgrass (*Zostera marina*), as described by Ghisalberti and Nepf.[38] The meadow was 6.5 m long and had a stem density of 230 plants m^{-2}. When undeflected, the meadow height was $h = 21.5$ cm (blade plus stem), and the frontal area per volume was $a = 5.2$ m^{-1}, assuming all blades were seen by the flow, so that the roughness density was $ah = 1.1$. This corresponds to a dense canopy ($ah > 0.1$) for which turbulent sweeps are not expected to penetrate through the entire height of the canopy.[10,45] For comparison, we also considered a completely rigid model canopy with comparable roughness density, $h = 13.8$ cm, $a = 8$ m^{-1}, and $ah = 1.1$ (run R8 in Ghisalberti and Nepf[14]).

Acoustic Doppler velocimetry (ADV) was used to measure the three velocity components (u, v, w) at four positions separated by 7.5 cm. At each point, vertical profiles were collected at 1-cm intervals over depth, using a record length of 10 min. A 12-cm space ($1.8\Delta S$, where ΔS is the average distance between stems) was made in the meadow to allow probe access without interference from blades. Ikeda and Kanazawa showed that the removal of canopy elements over a length less than $7\Delta S$ has little impact on flow statistics.[46] Given that our gap is smaller, we also expect the gap to have negligible impact on the velocity measurement (as discussed in detail by Ghisalberti and Nepf[14]). The Reynolds stress is defined as $\overline{u'w'}$. The maximum penetration of turbulence into the canopy was defined by the position at which the Reynolds stress dropped to 10% of the peak value observed at the top of the canopy. The distance to this point from the top of the canopy is called the penetration scale, δ_e. A video camera was used to determine the deflected meadow height h and *monami* amplitude A_w, defined by the vertical excursion of blades during a *monami* cycle (Table 1 in Ghisalberti and Nepf[14]). Using the standard deviation of the velocity record, σ_u, the skewness of u was defined as $Sk_u = \overline{u'^3}/\sigma_u^3$, and similarly for Sk_w. The turbulence statistics were first calculated for individual profiles and then averaged over four profiles at different locations within the meadow, using linear interpolation to match the vertical positions. The Cauchy number was estimated in two ways, to reflect both the impact of the surrounding canopy and the unsteady variation in the deflection of individual blades. A predictive equation for the time-averaged deflected height of a meadow (h), as a function of Ca and R_B (Eq. (4) in Luhar and Nepf[47]), was used to infer the value of Ca, based on the observed value of h, which we call Ca_h. For some flow conditions, the passage of shear-layer vortices generated an additional, time-varying deflection, called *monami*. Using the *monami* amplitude (A_w), a second estimation, Ca_{A_w}, was found using the canopy height at the point of maximum deflection ($h - A_w$) in Eq. (4) of Luhar and Nepf.[47] The second estimate captures the conditions associated with the strongest sweep events. Finally, to provide a direct comparison between skewness and Vogel number B, the value of $B = B(Ca)$ was extracted from the curve shown in Fig. 1(a) (Eq. (16) in Luhar and Nepf[31]), with $R_B = 6.4$, corresponding to the model seagrass. Because $Ca \propto U^2$, $C_D/C_D^o \propto Ca^{B/2}$, so that B is twice the slope of the curve.

B. Experimental results

To begin, we consider how the mean reconfiguration of the meadow impacts vertical profiles of mean velocity, Reynolds stress, and skewness (Fig. 2). We compare a case with negligible reconfiguration (F2; $h = 21.3$ cm, $A_w = 0$) to a case with weak reconfiguration (F5; $h = 17$ cm, $A_w = 4.1$ cm). For each profile, a horizontal line indicates the mean deflected height, h. Once reconfiguration was initiated, h progressively declined as the mean velocity at the top of the meadow ($\overline{u}_h$), and thus Ca, increased (Table I). The peak Reynolds stress coincided roughly with h, and thus descended toward the bed as the meadow was deflected (Fig. 2(b)). Note that Reynolds stress was linear above the meadow, consistent with open channel flow. The length-scale over which Reynolds stress penetrated into the meadow (δ_e) also increased with Ca, from 9.8 cm (F1) to 12.8 cm (F6, Table I), suggesting that with increasing mean reconfiguration the meadow also became more porous to the sweep events that carry most of the turbulent flux. The penetration of sweep events was also reflected in the *monami* amplitude (A_w), which also increased with increasing Ca (Table I). The increasing penetration length-scale and decreasing canopy height together caused the fraction of

TABLE I. Time-mean deflected canopy height h (cm above bed); *monami* amplitude A_w (dashed means no *monami* observed); time-mean velocity at top of canopy $\overline{u}_h$ (* as given in Table 1 of Ghisalberti and Nepf[14]). Undeflected meadow height is 21.5 cm. Penetration length-scale, δ_e, is distance from top of canopy to point at which Reynolds stress is reduced to 10% of maximum. Ca_h is Cauchy number estimated from time-mean deflected height (h) using Eq. (4) in Luhar and Nepf.[47] Ca_{A_w} uses maximum deflected height, $h - A_w$. Maximum magnitude of skewness values in u and w ($Sk_{u,\max}$ and $Sk_{w,\min}$) and vertical position of maximum skewness in u, $z(Sk_{u,\max})$, are the mean of values selected from four individual vertical profiles, and the uncertainty indicates one standard deviation between profile values.

	$h^\star$ [cm]	$A_w^\star$ [cm] ±25%	$\overline{u}_h^\star$ [cm s^{-1}]	δ_e [cm] ±1.0	δ_e/h ±0.5	Ca_h	Ca_{A_w}	$z(Sk_{u,\max})$ [cm]	$Sk_{u,\max}$	$Sk_{w,\min}$
F1	21.5	...	1.7	9.8	0.46	1	1	13 ± 2	0.72 ± 0.16	−1.26 ± 0.09
F2	21.3	...	3.0	10.0	0.51	2	2	14 ± 2	1.13 ± 0.16	−1.16 ± 0.21
F3	20.0	2.7	3.7	11.0	0.55	6	16	10 ± 2	1.37 ± 0.15	−1.43 ± 0.12
F4	18.6	3.5	4.4	11.5	0.62	10	31	10 ± 1	1.36 ± 0.06	−1.45 ± 0.12
F5	17.0	4.1	5.7	12.3	0.72	17	61	7 ± 2	1.60 ± 0.15	−1.18 ± 0.18
F6	15.5	4.4	7.9	12.8	0.83	28	122	7 ± 1	1.38 ± 0.13	−1.34 ± 0.27
R8	13.8	...	4.0	7.8	0.57	0	0	9 ± 1	0.78 ± 0.26	−0.96 ± 0.25

canopy influenced by vertical turbulent flux (δ_e/h) to increase with increasing Ca, from 0.46 (F1) to 0.83 (F6, Table I).

The increasing preference for large sweep events with increasing Ca is evident in the skewness profiles. For both cases shown (F2 and F5, Fig. 2), the skewness of u (Sk_u) was elevated in the upper canopy, but returned to zero in the lower canopy, suggesting that sweep events did not penetrate to the bed for either flow condition, and this is consistent with the penetration length-scale (Table I) and other observations in dense canopies (e.g., Chen *et al.*[48]). The peak Sk_u moved closer to the bed with increasing Ca (see $z(Sk_{u,\max})$ in Table I), due both to the deflection of the meadow (h) and the increase in penetration length (δ_e), i.e., similar to the Reynolds stress. Specifically, the peak Sk_u occurred at $z = 14$ cm (F2) and $z = 7$ cm (F5), with the distance from the meadow interface (h) increasing from 7.3 cm (F2) to 10 cm (F5). Similar trends were seen in Sk_w; however, the vertical skewness did not always return to zero near the bed. A similar tendency has been observed in terrestrial canopies.[18] The greater penetration of Sk_w relative to Sk_u may reflect a preferential

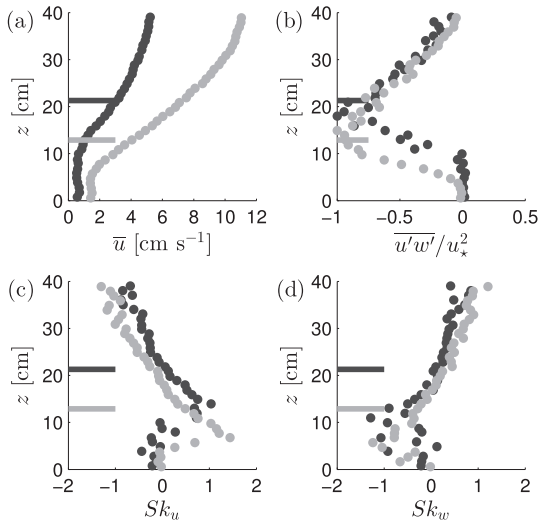

FIG. 2. Vertical profiles of (a) time-mean streamwise velocity ($\overline{u}$), (b) mean vertical momentum flux ($\overline{u'w'}$) normalized by the square of friction velocity ($u_\star^2$), (c) skewness of u (Sk_u), and (d) skewness of w (Sk_w) for two flow rates over a flexible canopy, one case with negligible reconfiguration (F2; black dots) and the other case with weak reconfiguration (F5; grey dots). Each profile is a spatial average of four individual profiles.[14] The solid horizontal lines indicate the canopy height h.

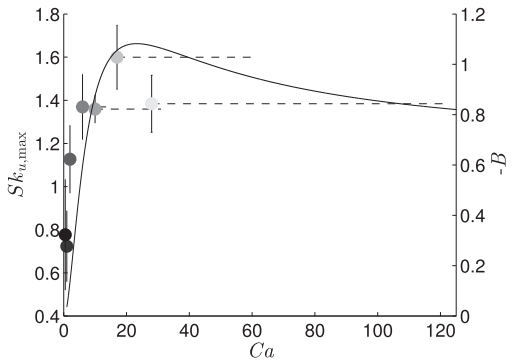

FIG. 3. Left-hand axis shows maximum skewness of u (Sk_u) observed within canopy for different values of Cauchy number, Ca. Circles indicate Ca_h and horizontal dashed lines extend to Ca_{A_w}, as defined in Table I. Vertical error bars represent the standard deviation between at least four individual profiles. Solid curve and right-hand axis show the value of Vogel exponent (plotted as $-B$) derived from the slope of the function C_D/C_D^o versus Ca shown in Fig. 1(a).

damping of the longitudinal velocity component relative to the vertical component, which may be due to asymmetries in the plant elements that produce asymmetries in the drag.

Finally, we consider how observed changes in peak skewness relate to the expected impact of reconfiguration on drag coefficient (Fig. 1). We anticipate that as the Vogel number (B) becomes increasingly negative, the difference between the drag coefficient acting on weak and strong events will become greater, $C_D \propto u^B$, with the result that stronger sweep events are increasingly favored, producing larger values of skewness. The Vogel number (plotted as $-B$ in Fig. 3) was derived from the slope of the function C_D/C_D^o versus Ca, shown in Fig. 1(a). A peak value of $-B = 1.1$ is observed at $Ca = 21$. As discussed with Fig. 1, this corresponds to the weak reconfiguration regime. For higher values of Ca (beyond that shown in Fig. 3), B asymptotes to the prediction for strong reconfiguration, $-B = 2/3$. The observed peak values of Sk_u are also shown in Fig. 3. Circles indicate Ca_h and horizontal dashed lines extend to Ca_{A_w}, as defined in Table I. The maximum skewness has a peak value at $Ca_h = 17$ (F5 in Table I), which is close to $Ca = 21$, the position at which B is the most negative. Note that the curve for $-B$ and the skewness points shown together in Fig. 3 are not directly related. In other words, we do not imply the line for $-B$ fits the points; we plot them together to visually reveal how the peak in $Sk_{u,\,\max}$ and $-B$ occur at similar values of Ca and within the regime of weak reconfiguration. We also note that for $Ca_h = 1$ (F1), the flexible canopy produces a skewness maximum ($Sk_{u,\,\max}$) that is the same as that observed in the rigid canopy (R8) within uncertainty, i.e., at $Ca = 1$ the flexible canopy interacts with the flow in analogy to a fully rigid canopy. Finally, it is interesting to note that field conditions for seagrass range from $Ca = 0$ (slack tide) to 2000 (based on values given in Table II and Fig. 7 of Luhar and Nepf[31]), so that all three regimes of behavior; rigid ($B = 0$), weak reconfiguration ($B < -1$), and strong reconfiguration ($B = -2/3$); are experienced by real meadows.

III. NUMERICAL SIMULATION OF PLANT RECONFIGURATION

In this section, we use a LES model to investigate the effects of different modes and degrees of plant reconfiguration on the turbulence characteristics inside a terrestrial canopy. The different modes and degrees of reconfiguration are modeled by varying the Vogel number B. We consider four cases: $B = 0$ (rigid canopy with no reconfiguration), $B = -2/3$ (strong reconfiguration for 1D linear elastic bending[29]), $B = -1$ (weak reconfiguration for 1D elastic bending described in Sec. II), and $B = -4/3$ (strong reconfiguration for two-dimensional (2D) linear elastic bending[33]).

A. Numerical model

The LES model employed here is described in detail by Pan *et al.*[26] The sink of flow momentum per unit volume induced by forces acting on the surfaces of canopy elements is parameterized as a

"drag force" ($\boldsymbol{f}_D$) following the approach proposed by Shaw and Schumann,[20]

$$\boldsymbol{f}_D = -C_D\,(a_c\mathbf{P})\cdot(|\tilde{\boldsymbol{u}}|\tilde{\boldsymbol{u}})\,, \tag{4}$$

where $\tilde{\boldsymbol{u}}$ is the filtered velocity, and a_c is the two-sided leaf area density. Note that in Sec. II the frontal area per volume a is equivalent to one-sided leaf area density, and the roughness density ah is equivalent to one-sided leaf area index (LAI). The projection tensor $\mathbf{P} = P_x\boldsymbol{e}_x\boldsymbol{e}_x + P_y\boldsymbol{e}_y\boldsymbol{e}_y + P_z\boldsymbol{e}_z\boldsymbol{e}_z$ is used to split a_c into streamwise (x), spanwise (y), and vertical (z) directions, where $\boldsymbol{e}_j$ is the unit vector in the jth direction. Values of a_c and $\mathbf{P}$ are provided by Pan *et al.*[26] Please note the distinction between the volume average ($\boldsymbol{f}_D$) and the drag on a single blade (F_D) defined by Eq. (1).

LES studies of forests[20–24,49] and crop canopies[25,50] typically treat C_D as a constant, implying $|\boldsymbol{f}_D| \propto |\tilde{\boldsymbol{u}}|^2$. To reflect the impact of reconfiguration, the general expression $C_D = (U/A)^B$ was adopted, with $|\tilde{\boldsymbol{u}}|$ being the characteristic velocity scale U. Here, A is a velocity scale related to canopy geometry and rigidity,[26] and B is the Vogel number. The dependence of C_D on velocity can be estimated by fitting field experimental data to the mean momentum equation following the approach used by Cescatti and Marcolla.[51] Fitting C_D to data obtained in a large maize field near Mahomet, IL on July 10, 2011 ($h = 2.1$ m, LAI = 3.3, and for details of field experiment see Gleicher *et al.*[52]), Pan *et al.* obtained $A = 0.29$ m s^{-1} and $B = -0.74$.[26] This estimated Vogel exponent is within the range of theoretical values ($B = -2/3$ to $-4/3$) and other measured values ($B = -0.5$ to -0.8), described in Sec. I. Pan *et al.*[26] compared LES results using the velocity-dependent drag coefficient model to those using the constant drag coefficient model ($C_D = 0.25$, based on the data obtained by Wilson *et al.*[53]). Note that a constant drag coefficient assumes no reconfiguration ($B = 0$). The drag model that mimicked the impact of reconfiguration produced a remarkable improvement in the comparison between LES results and observed values of skewness (reducing the underprediction of Sk_u and Sk_w from 60% to 5% and 20%, respectively) and the stress fraction carried by strong sweep events (reducing the underprediction from 40% to 5%).

In this work, an upper limit ($C_{D,\,\max} = 0.8$, as suggested by the same experimental data) is used to cap the drag coefficient, reflecting the asymptotic regime of negligible reconfiguration in the limit of $\overline{u} \to 0$. LES runs are conducted using the constant drag coefficient model ($C_D = 0.28$, $B = 0$; case (1)) and the revised reconfiguration drag model (velocity-dependent drag coefficient model),

$$C_D = \min\left((|\tilde{\boldsymbol{u}}|/A)^B, C_{D,\max}\right), \tag{5}$$

considering a wide range of reconfiguration behavior, specifically, for cases (2) $A = 0.22$ m s^{-1}, $B = -2/3$, (3) $A = 0.38$ m s^{-1}, $B = -1$, and (4) $A = 0.48$ m s^{-1}, $B = -4/3$. In each of these four cases, the value of B is prescribed, and the values of C_D and A are found by fitting the experimental data. Recall that an increasingly negative value of B preferentially enhances the penetration of strong events into the canopy. In the fitting procedure, each value of C_D is weighted by the inverse of the velocity squared, so that higher weight is given to events of higher velocity, i.e., the conditions for which reconfiguration has the most impact on drag coefficient. Fig. 4 compares drag coefficient models with experimental data. The velocity-dependent drag coefficient model presents a similar shape to the theoretical model depicted in Fig. 1(a). Beginning at 0.3–0.6 m s^{-1}, C_D decreases with increasing velocity, and with higher dependence given by more negative values of B. In particular, note that in the high velocity range ($|\tilde{\boldsymbol{u}}| > 1.5$ m s^{-1}), C_D decreases with increasingly negative value of B, corresponding to an increased tendency for reconfiguration to reduce the drag experienced by stronger events. However, for the low velocity range ($|\tilde{\boldsymbol{u}}| < 1$ m s^{-1}), this trend is reversed, with C_D larger for more negative values of B.

B. Simulation results

LES results of turbulence statistics are compared with field experimental data computed using a period of 7.5 h (0930-1700 CDT) of steady turbulence obtained on July 10, 2011 near Mahomet, IL (dots indicating the average and error bars indicating the standard deviation for 30-min intervals in Figs. 5 and 6). Data obtained by Wilson *et al.*[53] (crosses in Fig. 5) are also shown as a consistency check, because the canopy type and structure are similar in both datasets. In addition to vertical profiles of turbulence statistics, mechanisms of momentum transport inside the canopy are

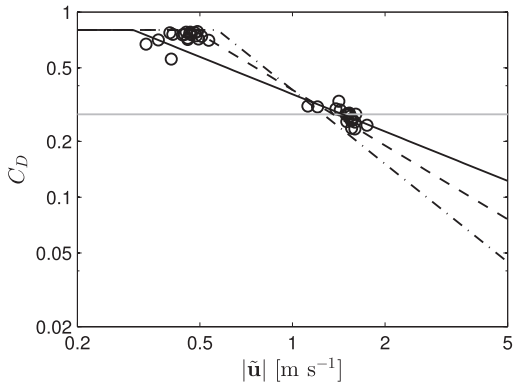

FIG. 4. Drag coefficient (C_D) against the magnitude of filtered velocity scale ($\tilde{\boldsymbol{u}}$) fitted using field experimental data (circles) and the models C_D = constant (*grey line*) and $C_D = \min\left((|\tilde{\boldsymbol{u}}|/A)^B, C_{D,\max}\right)$ (Eq. (5); black lines). Grey solid and black solid, dashed, and dashed-dotted lines indicate cases (1) $C_D = 0.28$, $B = 0$, (2) $A = 0.22$ m s^{-1}, $B = -2/3$, (3) $A = 0.38$ m s^{-1}, $B = -1$, and (4) $A = 0.48$ m s^{-1}, $B = -4/3$, respectively.

investigated using the quadrant analysis proposed by Lu and Willmarth.[54] Following the standard practices in LES studies, the mean stress $\overline{u'w'}$ (and consequently the friction velocity $u_\star = \sqrt{|\overline{u'w'}|_h}$) is determined using the resolved and subgrid-scale (SGS) parts. Standard deviations and skewness of velocity fluctuations are determined based only on the resolved scales. The vertical momentum flux is decomposed into four quadrants. Events in the first quadrant ($u' > 0$, $w' > 0$) are outward interactions, events in the second quadrant ($u'\langle 0$, $w'\rangle 0$) are ejections, events in the third quadrant ($u' < 0$, $w' < 0$) are inward interactions, and events in the fourth quadrant ($u' > 0$, $w' < 0$) are sweeps.[55] $S_{i,H}$ indicates the momentum flux carried by events in the ith quadrant that are H times stronger than the mean ($|u'w'|/|\overline{u'w'}| > H$); $S^f_{i,H} = S_{i,H}/|\overline{u'w'}|$ indicates the stress fractions carried by these events; and $S^f_H = \Sigma^4_{i=1} S^f_{i,H}$ indicates the stress fractions carried by all events that are H times stronger than the mean. In this analysis, the SGS component of the vertical momentum flux is excluded.

In Fig. 5(a), predictions of the streamwise component of time-averaged drag, $\overline{f}_{D,x}$, is negative for all four cases. The vertical integration of $\overline{f}_{D,x}$ is held approximately constant (with less than 0.5% difference across all cases), because parameters in the model $C_D = C_D(|\tilde{\boldsymbol{u}}|)$ (i.e., A and B in Eq. (5)) are fitted using the measured profile of mean vertical momentum flux (see Fig. 4). Increasingly negative values of B decrease the magnitude of $\overline{f}_{D,x}$ in the upper 20% of the canopy, where velocity falls in the high velocity range, and increase the magnitude of $\overline{f}_{D,x}$ in the lower 80% of the canopy, where velocity falls in the low velocity range. In Fig. 5(b), predictions of normalized, time-mean velocity, $\overline{u}/\overline{u}_h$, resulting from drag models with $B \neq 0$ (black lines) are distinct from those with $B = 0$ (grey line), showing better agreement with measurements inside the canopy. Specifically, using a constant C_D (assuming $B = 0$, no reconfiguration) produces an overestimation of the mean velocity inside the canopy by 100%. For second-order moments, increasingly negative values of B only slightly increases the downward momentum flux ($|\overline{u'w'}|$; Fig. 5(c)) and the standard deviation of u (σ_u; Fig. 5(e)). In other words, ignoring the effect of reconfiguration by assuming a constant C_D leads to only a slightly shallower estimation of the penetration of momentum into the canopy layer, consistent with the findings of Wilson *et al.*[53] The effects of reconfiguration on the standard deviation of v (σ_v; not shown) and w (σ_w; Fig. 5(f)) are negligible, implying that reconfiguration affects mostly the energy contained in the streamwise direction rather than spanwise or vertical directions.

The effects of the mode of reconfiguration, characterized by the negative value of B, are most pronounced for the sweep-ejection ratio ($S_{4,0}/S_{2,0}$; Fig. 5(d)) and the skewness of u (Sk_u; Fig. 5(g)) and w (Sk_w; Fig. 5(h)), with the magnitude of all three statistics increasing with increasingly negative B. The increasing magnitude of skewness arises directly from the reduction in drag coefficient with increasing velocity, which, as mentioned in Sec. I, allows stronger events to penetrate more easily

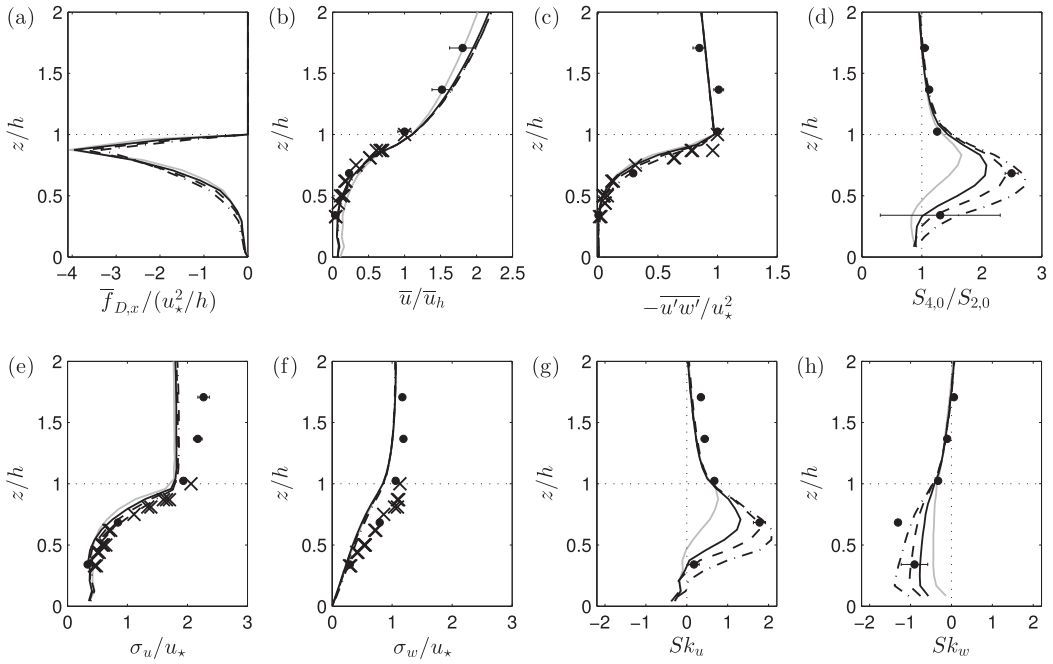

FIG. 5. LES results of (a) normalized streamwise component of mean drag ($\overline{f}_{D,x}/\left(u_\star^2/h\right)$), (b) normalized mean velocity ($\overline{u}/\overline{u}_h$), (c) normalized mean vertical momentum flux ($-\overline{u'w'}/u_\star^2$), (d) ratio between stress fractions carried by sweeps and ejections ($S_{4,0}/S_{2,0}$), (e) normalized standard deviation of u ($\sigma_u/u_\star$), (f) normalized standard deviation of w ($\sigma_w/u_\star$), (g) skewness of u (Sk_u), and (h) skewness of w (Sk_w) against normalized height (z). Here, $u_\star$ is the friction velocity, and h is the canopy height. Simulation results (lines, see Fig. 4 for representations) are evaluated against field experimental data (symbols). Dots with error bars indicate average and standard deviation for 30-min intervals of data obtained during 0900-1730 CDT on 10 July 2011 in a large maize field near Mahomet, IL,[26,52] and crosses indicate data obtained by Wilson *et al.*[53] The canopy type and structure are similar in both datasets.

into the canopy. For example, at $z/h = 2/3$, the stress fraction carried by events eight times stronger than the mean magnitude ($H = 8$) increases from 27% for $B = 0$ to 50% for $B = -1$ (Fig. 6(a)). As B becomes more negative, the deeper penetration of stronger events also makes the peak of Sk_u move towards the ground (Fig. 5(g)). Sweep events are associated with elevated streamwise velocity ($u' > 0$), and thus receive a preference in regimes for which C_D decreases with increasing U, becoming stronger when B is more negative. At $z/h = 2/3$, for example, the stress fractions carried by sweep events increase from 75% ($B = 0$) to 85% ($B = -1$) for $H = 0$ and from 25% ($B = 0$) to 50% ($B = -1$) for $H = 8$ (Fig. 6(c)). The enhancement in stress fractions increases with the strength of sweep events, showing that events with strong positive u' (large u and consequently large U) are preferentially allowed to penetrate the canopy by reconfiguration. On the other hand, ejection events associated with weaker streamwise velocity ($u' < 0$) are preferentially damped in this regime, and

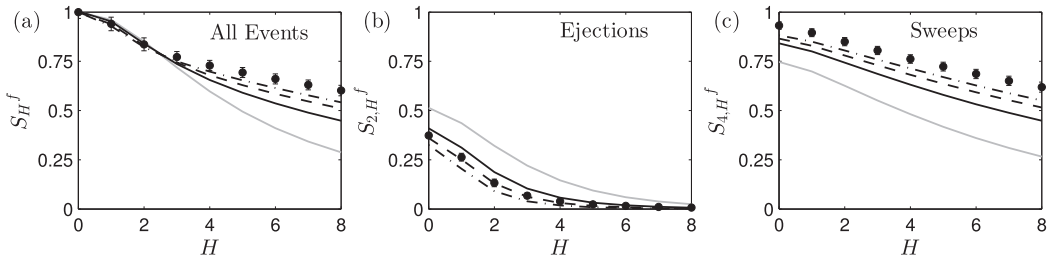

FIG. 6. Comparison of LES results and field experimental data of stress fractions carried by (a) all events (S_H^f), (b) ejections ($S_{2,H}^f$), and (c) sweeps ($S_{4,H}^f$) against hole size (H) at $z/h = 2/3$. See Fig. 5 for representations of lines and symbols.

thus become weaker when B is more negative. At $z/h = 2/3$, for example, the stress fractions carried by ejection events decrease from 50% ($B = 0$) to 35% ($B = -1$) for $H = 0$ and from 15% ($B = 0$) to negligible ($B = -1$) for $H = 4$ (Fig. 6(b)). The reduction of stress fractions occurs mostly for strong ejection events ($H \geq 4$), because ejections originate in the bottom of the canopy where lower velocity is associated with higher C_D (i.e., higher damping). The increase in sweeps and decrease in ejections both lead to the increase in the sweep-ejection ratio (Fig. 5(d)). The overall best agreement with observations across skewness and quadrant analysis occurs for $B = -1$ (black dashed lines in Figs. 5(d), 5(g), 5(h), and 6). Note that when B is fitted to data, Pan *et al.*[26] obtained $B = -0.74$. However, as seen in Fig. 4, the points calculated from the data do not constrain the fit very tightly. A new fit, which more heavily weights the large velocity portion of the data (which is more reliably measured in the field), yields $B = -0.83$. The idea that the reconfiguration of the maize plants falls in the regime of weak reconfiguration for the 1D elastic case (described in Sec. II) seems perfectly reasonable, because the simple bending observed in the field does not display deflection beyond the posture in Fig. 1(b).

IV. CONCLUSIONS

Results obtained from laboratory and numerical experiments demonstrate that concepts developed for mean reconfiguration can be extended to instantaneous reconfiguration, at least for time-scales over which the plant can respond. This provides a link between plant reconfiguration and turbulence dynamics. Although the laboratory and numerical experiments are quite different (e.g., in LAI, geometry, density, rigidity of the canopy, density of the fluid, and the rate of the flow), they show similar effects of Vogel number B on the velocity skewness. In particular, as the Vogel number becomes more negative, the peak Sk_u increases in magnitude. Specifically, LES of a maize canopy gives $Sk_{u,\,\max}$ of 0.8, 1.3, and 1.8 when B is specified to be 0, $-2/3$, and -1, respectively (Fig. 5(g)). Similarly, for the model seagrass meadow, the highest value of peak skewness ($Sk_{u,\,\max} = 1.60$, F5) occurs at the conditions associated with the most negative value of B (Fig. 3). In addition, as peak skewness (Sk_u) increases with more negative B, the peak skewness also penetrates deeper into the canopy (lower values of $z(Sk_{u,\,\max})/h$), as inferred from Table I and Fig. 5(d). Note that reconfiguration is not the only mechanism that affects skewness. For example, in a canopy of steel cylinders (no reconfiguration) the value of $Sk_{u,\,\max}$ increased from negligible to 0.8 when LAI was increased from 0.03 to 0.5.[56] In an orchard forest canopy, the value of $Sk_{u,\,\max}$ decreased from 1 to negligible when the atmospheric temperature stratification condition changed from neutral to free convection.[57] Our results show that, if other conditions remain unchanged, more negative values of B lead to a greater penetration of sweeps ($u' > 0$, $w' < 0$) and larger values of Sk_u. In submerged aquatic canopies, the penetration of strong sweeps to the bed could significantly elevate resuspension, so that reconfiguration (changes in B) may impact water clarity and particle retention within the bed. Further, the sweeps originating at the top of the canopy are associated with the KH coherent structures in the canopy-shear layer, so that these results are saying that plant reconfiguration may enhance the influence of these coherent structures on turbulent transport into the canopy. These modifications will certainly influence the turbulent transport of scalars and particles within the canopy, modulating the fluxes across the canopy-atmosphere or canopy-free stream interfaces. The increased dominance of sweeps over ejections in canopies with larger Vogel number is expected to favor transport of air pollutants and aerosols into vegetated regions, likely increasing the efficiency of these canopies in removing these pollutants from the atmosphere. However, further work is necessary to establish and quantify the potential impacts of canopy reconfiguration on fluxes of sensible heat, water vapor, and carbon dioxide.

For one-dimensional linear elastic reconfiguration, we highlight the importance of weak reconfiguration, which is the transition between the asymptotic regimes of negligible reconfiguration ($B = 0$) and strong reconfiguration ($B = -2/3$). In the weak reconfiguration regime, the bending length-scale is smaller than the drag length-scale, leading to a stronger dependence between drag coefficient and velocity than that observed during strong reconfiguration. In other words, the Vogel exponent is more negative ($B < -2/3$) in the weak reconfiguration regime, reaching a peak value of $B = -1.1$ at $Ca = 21$. Importantly, because weak reconfiguration produces the most negative

Vogel exponents, it also produces the strongest impact on skewness. All three regimes, including weak reconfiguration, are observed in the model seagrass meadow, and are likely present in natural canopies in which simple bending is observed, like seagrasses, stems, branches, maize, and wheat. Gosselin *et al.*[33] described a similar intermediate regime of bending for plates and disks. For strong reconfiguration, the Vogel exponent has been shown to be more negative for 2D bending ($B = -4/3$) than for 1D bending ($B = -2/3$)[29,30] and, as our LES results show, the 2D regime results in the largest predictions of skewness. A wide range of broad leaves can fold into cones and experience 2D reconfiguration, and thus enter the $-4/3$ regime.[58] Many terrestrial canopies have a Vogel number between $-2/3$ and $-4/3$,[28,30] suggesting that the classes of 1D and 2D reconfiguration identified by previous researchers for flexible strips, plates, and disks can be used to describe the reconfiguration of many plant canopies. However, a greater refinement of models may be needed for more complex plant geometries, and an exploration of the impact of canopy density on reconfiguration is also needed.

With the vertically integrated mean drag force held approximately constant, changing the mode of the reconfiguration (characterized by the Vogel number, B) has a strong impact on the mechanisms of momentum transport. The mean vertical momentum flux remains approximately the same, but the distribution, strength, and fractions of momentum carried by sweeps ($u' > 0$, $w' < 0$) and ejections ($u' < 0$, $w' > 0$) are altered significantly. Using a constant drag coefficient is capable of reproducing vertically integrated sink of momentum within the canopy layer, and consequently the first- and second-order turbulence statistics. However, accounting for the effect of reconfiguration is essential to reproduce the distribution of the momentum sink between weak ($u' < 0$) and strong ($u' > 0$) events. Therefore, higher order moments such as skewness, as well as the fractions of momentum transported by sweeps and ejections, are very sensitive to reconfiguration. These results confirm the inadequacy of describing the effects of canopy-scale coherent structures using just first- and second-order turbulence statistics. The current understanding of canopy turbulence is based on relating the properties of coherent structures to the mean drag force exerted by the canopy (one example is the penetration depth studied by Ghisalberti and Nepf[14]). Perhaps, further advances will result from understanding the drag reduction by reconfiguration and its effects on instantaneous turbulence structure.

ACKNOWLEDGMENTS

This research is supported by the National Science Foundation (NSF) Grant No. AGS1005363.

[1] S. B. Verma, D. D. Baldocchi, D. E. Anderson, D. R. Matt, and R. J. Clement, "Eddy fluxes of CO_2, water vapor, and sensible heat over a deciduous forest," Bound.-Layer Meteorol. **36**, 71–91 (1986).
[2] D. Baldocchi, "A Lagrangian random-walk model for simulating water vapor, CO_2 and sensible heat flux densities and scalar profiles over and within a soybean canopy," Bound.-Layer Meteorol. **61**, 113–144 (1992).
[3] J. D. Fuentes, T. J. Gillespie, G. Den Hartog, and H. H. Neumann, "Ozone deposition onto a deciduous forest during dry and wet conditions," Agric. For. Meteorol. **62**, 1–18 (1992).
[4] E. Lamaud, A. Carrara, Y. Brunet, A. Lopez, and A. Druilhet, "Ozone fluxes above and within a pine forest canopy in dry and wet conditions," Atmos. Environ. **36**, 77–88 (2002).
[5] S. E. Lindberg, T. P. Meyers, G. E. Taylor, R. R. Turner, and W. H. Schroeder, "Atmosphere-surface exchange of mercury in a forest: Results of modeling and gradient approaches," J. Geophys. Res. **97**, 2519–2528, doi:10.1029/91JD02831 (1992).
[6] G. Buzorius, Ü. Rannik, J. M. Mäkelä, T. Vesala, and M. Kulmala, "Vertical aerosol particle fluxes measured by eddy covariance technique using condensational particle counter," J. Aerosol Sci. **29**, 157–171 (1998).
[7] F. Di-Giovanni and P. G. Kevan, "Factors affecting pollen dynamics and its importance to pollen contamination: A review," Can. J. For. Res. **21**, 1155–1170 (1991).
[8] R. Nathan, G. G. Katul, H. S. Horn, S. M. Thomas, R. Oren, R. Avissar, S. W. Pacala, and S. A. Levin, "Mechanisms of long-distance dispersal of seeds by wind," Nature (London) **418**, 409–413 (2002).
[9] D. E. Aylor, "The role of intermittent wind in the dispersal of fungal pathogens," Annu. Rev. Phytopathol. **28**, 73–92 (1990).
[10] M. Luhar, J. Rominger, and H. Nepf, "Interaction between flow, transport and vegetation spatial structure," Environ. Fluid Mech. **8**, 423–439 (2008).
[11] S. E. Lawson, K. J. McGlathery, and P. L. Wiberg, "Enhancement of sediment suspension and nutrient flux by benthic macrophytes at low biomass," Mar. Ecol. Prog. Ser. **448**, 259–270 (2012).
[12] M. M. van Katwijk, A. R. Bos, D. C. R. Hermus, and W. Suykerbuyk, "Sediment modification by seagrass beds: Muddification and sandification induced by plant cover and environmental conditions," Estuar. Coast. Shelf Sci. **89**, 175–181 (2010).

[13] M. R. Raupach, J. J. Finnigan, and Y. Brunet, "Coherent eddies and turbulence in vegetation canopies: The mixing-layer analogy," Bound.-Layer Meteorol. **78**, 351–382 (1996).
[14] M. Ghisalberti and H. Nepf, "The structure of the shear layer in flows over rigid and flexible canopies," Environ. Fluid Mech. **6**, 277–301 (2006).
[15] R. H. Shaw, J. Tavangar, and D. P. Ward, "Structure of the Reynolds stress in a canopy layer," J. Clim. Appl. Meteorol. **22**, 1922–1931 (1983).
[16] M. Ghisalberti and H. Nepf, "Mass transport in vegetated shear flows," Environ. Fluid Mech. **5**, 527–551 (2005).
[17] C. Thomas and T. Foken, "Flux contribution of coherent structures and its implications for the exchange of energy and matter in a tall spruce canopy," Bound.-Layer Meteorol. **123**, 317–337 (2007).
[18] J. J. Finnigan, "Turbulence in plant canopies," Annu. Rev. Fluid Mech. **32**, 519–571 (2000).
[19] T. P. Meyers and D. D. Baldocchi, "The budgets of turbulent kinetic energy and Reynolds stress within and above a deciduous forest," Agric. For. Meteorol. **53**, 207–222 (1991).
[20] R. H. Shaw and U. Schumann, "Large-eddy simulation of turbulent flow above and within a forest," Bound.-Layer Meteorol. **61**, 47–64 (1992).
[21] H. B. Su, R. H. Shaw, K. T. Paw, C. H. Moeng, and P. P. Sullivan, "Turbulent statistics of neutrally stratified flow within and above a sparse forest from large-eddy simulation and field observations," Bound.-Layer Meteorol. **88**, 363–397 (1998).
[22] E. G. Patton, P. P. Sullivan, and K. J. Davis, "The influence of a forest canopy on top-down and bottom-up diffusion in the planetary boundary layer," Q. J. R. Meteorol. Soc. **129**, 1415–1434 (2003).
[23] S. Dupont and Y. Brunet, "Influence of foliar density profile on canopy flow: A large-eddy simulation study," Agric. For. Meteorol. **148**, 976–990 (2008).
[24] K. Gavrilov, D. Morvan, G. Accary, D. Lyubimov, and S. Meradji, "Numerical simulation of coherent turbulent structures and of passive scalar dispersion in a canopy sublayer," Comput. Fluids **78**, 54–62 (2013).
[25] W. Yue, M. B. Parlange, C. Meneveau, W. Zhu, R. Van Hout, and J. Katz, "Large-eddy simulation of plant canopy flows using plant-scale representation," Bound.-Layer Meteorol. **124**, 183–203 (2007).
[26] Y. Pan, M. Chamecki, and S. A. Isard, "Large-eddy simulation of turbulence and particle dispersion inside the canopy roughness sublayer," J. Fluid Mech. **753**, 499–534 (2014).
[27] S. Vogel, "Drag and flexibility in sessile organisms," Am. Zool. **24**, 37–44 (1984).
[28] B. Gaylord, C. A. Blanchette, and M. W. Denny, "Mechanical consequences of size in wave-swept algae," Ecol. Monogr. **64**, 287–313 (1994).
[29] S. Alben, M. Shelley, and J. Zhang, "Drag reduction through self-similar bending of a flexible body," Nature (London) **420**, 479–481 (2002).
[30] E. de Langre, A. Gutierrez, and J. Cossé, "On the scaling of drag reduction by reconfiguration in plants," C. R. Mec. **340**, 35–40 (2012).
[31] M. Luhar and H. M. Nepf, "Flow-induced reconfiguration of buoyant and flexible aquatic vegetation," Limnol. Oceanogr. **56**, 2003–2017 (2011).
[32] S. Alben, M. Shelley, and J. Zhang, "How flexibility induces streamlining in a two-dimensional flow," Phys. Fluids **16**, 1694–1713 (2004).
[33] F. Gosselin, E. de Langre, and B. Machado-Almeida, "Drag reduction of flexible plates by reconfiguration," J. Fluid Mech. **650**, 319–341 (2010).
[34] I. Albayrak, V. Nikora, O. Miler, and M. O'Hare, "Flow-plant interactions at a leaf scale: Effects of leaf shape, serration, roughness and flexural rigidity," Aquat. Sci. **74**, 267–286 (2012).
[35] D. L. Harder, O. Speck, C. L. Hurd, and T. Speck, "Reconfiguration as a prerequisite for survival in highly unstable flow-dominated habitats," J. Plant Growth Regul. **23**, 98–107 (2004).
[36] A. Koizumi, J. Motoyama, K. Sawata, Y. Sasaki, and T. Hirai, "Evaluation of drag coefficients of poplar-tree crowns by a field test method," J. Wood Sci. **56**, 189–193 (2010).
[37] J. J. Finnigan, "Turbulence in waving wheat," Bound.-Layer Meteorol. **16**, 181–211 (1979).
[38] M. Ghisalberti and H. M. Nepf, "Mixing layers and coherent structures in vegetated aquatic flows," J. Geophys. Res. **107**, 3-1–3-11, doi:10.1029/2001JC000871 (2002).
[39] S. E. Belcher, N. Jerram, and J. C. R. Hunt, "Adjustment of a turbulent boundary layer to a canopy of roughness elements," J. Fluid Mech. **488**, 369–398 (2003).
[40] J. Rominger and H. M. Nepf, "Flow adjustment and interior flow associated with a rectangular porous obstruction," J. Fluid Mech. **680**, 636–659 (2011).
[41] M. A. Abdelrhman, "Modeling coupling between eelgrass *Zostera marina* and water flow," Mar. Ecol. Prog. Ser. **338**, 81–96 (2007).
[42] M. W. Denny, B. P. Gaylord, and E. A. Cowen, "Flow and flexibility. II. The roles of size and shape in determining wave forces on the bull kelp *Nereocystis luetkeana*," J. Exp. Biol. **200**, 3165–3183 (1997).
[43] H. L. Stewart, "Morphological variation and phenotypic plasticity of buoyancy in the macroalga *Turbinaria ornata* across a barrier reef," Marine Biol. **149**, 721–730 (2006).
[44] B. Statzner, N. Lamouroux, V. Nikora, and P. Sagnes, "The debate about drag and reconfiguration of freshwater macrophytes: Comparing results obtained by three recently discussed approaches," Freshwater Biol. **51**, 2173–2183 (2006).
[45] H. M. Nepf, "Flow and transport in regions with aquatic vegetation," Annu. Rev. Fluid Mech. **44**, 123–142 (2012).
[46] S. Ikeda and M. Kanazawa, "Three-dimensional organized vortices above flexible water plants," J. Hydraul. Eng. **122**, 634–640 (1996).
[47] M. Luhar and H. M. Nepf, "From the blade scale to the reach scale: A characterization of aquatic vegetative drag," Adv. Water Resour. **51**, 305–316 (2013).
[48] Z. Chen, C. Jiang, and H. Nepf, "Flow adjustment at the leading edge of a submerged aquatic canopy," Water Resour. Res. **49**, 5537–5551, doi:10.1002/wrcr.20403 (2013).

[49] T. V. Prabha, M. Y. Leclerc, and D. Baldocchi, "Comparison of in-canopy flux footprints between large-eddy simulation and the Lagrangian simulation," J. Appl. Meteorol. Climat. **47**, 2115–2128 (2008).
[50] M. Kanda and M. Hino, "Organized structures in developing turbulent flow within and above a plant canopy, using a large eddy simulation," Bound.-Layer Meteorol. **68**, 237–257 (1994).
[51] A. Cescatti and B. Marcolla, "Drag coefficient and turbulence intensity in conifer canopies," Agric. For. Meteorol. **121**, 197–206 (2004).
[52] S. C. Gleicher, M. Chamecki, S. A. Isard, Y. Pan, and G. G. Katul, "Interpreting three-dimensional spore concentration measurements and escape fraction in a crop canopy using a coupled Eulerian-Lagrangian stochastic model," Agric. For. Meteorol. **194**, 118–131 (2014).
[53] J. D. Wilson, D. P. Ward, G. W. Thurtell, and G. E. Kidd, "Statistics of atmospheric turbulence within and above a corn canopy," Bound.-Layer Meteorol. **24**, 495–519 (1982).
[54] S. S. Lu and W. W. Willmarth, "Measurements of the structure of the Reynolds stress in a turbulent boundary layer," J. Fluid Mech. **60**, 481–511 (1973).
[55] W. W. Willmarth, "Structure of turbulence in boundary layers," Adv. Appl. Mech. **15**, 159–254 (1975).
[56] D. Poggi, A. Porporato, L. Ridolfi, J. D. Albertson, and G. G. Katul, "The effect of vegetation density on canopy sub-layer turbulence," Bound.-Layer Meteorol. **111**, 565–587 (2004).
[57] S. Dupont and E. G. Patton, "Influence of stability and seasonal canopy changes on micrometeorology within and above an orchard canopy: The CHATS experiment," Agric. For. Meteorol. **157**, 11–29 (2012).
[58] L. A. Miller, A. Santhanakrishnan, S. Jones, C. Hamlet, K. Mertens, and L. Zhu, "Reconfiguration and the reduction of vortex-induced vibrations in broad leaves," J. Exp. Biol. **215**, 2716–2727 (2012).